Probabilistic Analysis of Electric Vehicle Energy Consumption Using MPC Speed Control and Nonlinear Battery Model

Jun Chen
ECE, Oakland University
Rochester, MI 48309, USA
Email: junchen@oakland.edu

Man Liang
UniSA STEM, Univ. of South Australia
Adelaide, 5000, Australia
Email: annie.liang@unisa.edu.au

Xu Ma
Optimization and Control Group, PNNL
Richland, WA 99352, USA
Email: xu.ma@pnnl.gov

2021 IEEE Green Technologies Conference (GreenTech) | 978-1-7281-9139-3/21/$31.00 ©2021 IEEE | DOI: 10.1109/GREENTECH48523.2021.00038

***Abstract*—This paper conducts a probabilistic analysis of energy consumption of electric vehicle. In particular, the vehicle speed is controlled by a model predictive control (MPC) to follow given reference speed while minimizing energy consumption, and the battery is modeled by nonlinear dynamic equations. Speed tracking accuracy and energy economy of MPC speed control is evaluated on EPA Federal Test Procedure driving cycle, which is commonly used for city driving testing and includes an approximate driving distance of 17.77 km. Furthermore, to conduct probabilistic analysis, Monte Carlo approach is taken to simulate a total number of ten thousands of synthetic FTP driving cycles, each with different profile. Numerical results and conclusion are then drawn to confirm the robustness of MPC speed control and the environmental friendliness of electric vehicle. Insights on battery operations for maximum energy efficiency are also discussed.**

I. Introduction

Model predictive control (MPC) can deal with linear and nonlinear dynamical systems while keeping states and input within specified regions. Due to such flexibility and capability, MPC has been one of the most popular control methods [1], and has been applied to vehicle systems [2]–[4], smart grids [5], power converters [6], and communications [7], etc. For each control loop, MPC solves a constrained optimization problem using prediction over a finite horizon based on a dynamical model. Theoretical properties of MPC have also been studied in literature, concerning its stability, robustness, and feasibility

Recent efforts have been focused on applying MPC in automotive embedded systems. For example, [8] applied MPC for vehicle speed control in the context of connected and automated vehicle (CAV), particularly for heavy-duty vehicle platoon where the pedal information of lead vehicle is available to ego vehicles. Reference [9] applies speed profile shaping before MPC in order to reduce excessive acceleration and deceleration, while similar approach is taken in [10] that used a speed planar to ensure ride comfort. Besides longitudinal speed control, MPC has also been successful in lateral vehicle dynamics control and energy management. For example, [11], [12] applied MPC to optimize energy management in electric vehicle (EV). Reference [4] used MPC to coordinate steering and braking inputs for vehicle stability control, while [13] adopted MPC for simultaneous longitudinal and lateral control. MPC has also been investigated for possible usage in active safety [14].

After developing an MPC design for a given control problem, its performance and correctness are often demonstrated through simulation or experiment under specific maneuvers. Such approach, however, does not provide insights on the robustness with respect to different maneuvers. To alleviate this and to enhance MPC applicability, researchers have conducted investigation to incorporate *a prior* knowledge about the disturbance distribution into MPC design to guarantee robustness [15], [16], to cast the problem of finding control systems flaws into a optimal control problem [17], and to conduct stochastic sampling over control systems parameter space [18], [19].

Despite these promising research findings, a *probabilistic* analysis of MPC for longitudinal speed control is missing, leading to lack of insights on the average/worst/best MPC performance on a given cycle. In this paper, we address this limitation by using Monte Carlo approach. Firstly, we consider the vehicle longitudinal speed tracking problem, where MPC optimizes wheel torque inputs in order to track the given speed profile while minimizing energy consumption. Secondly, a higher fidelity model is then used as simulation plant, hence creating a model mismatch between MPC prediction model and virtual vehicle. Finally, Monte Carlo approach is taken to simulate a total number of ten thousands synthetic FTP driving cycles, each with different profile, to investigate the robustness of MPC design. Compared to aforementioned work [15]–[17], this work does not aim at designing a robust MPC against known disturbance distribution, but rather to demonstrate and quantify the robustness of a given MPC design through simulation.

The rest of this paper is organized as follows. Section II introduces the vehicle dynamics model, together with the nonlinear battery model, which will be used as virtual plant for simulation. Section III presents the MPC speed control, while numerical results are discussed in Section IV. The paper is concluded in Section V.

2166-5478/21/$31.00 ©2021 IEEE
DOI 10.1109/GreenTech48523.2021.00038

Parameter	Value
B	10
C	1.9
D	1
E	0.97

TABLE I
PARAMETERS FOR MAGIC FORMULA (2).

Variable	Typical value
ρ	$1.225\ kg/m^3$
C_d	$0.25\ \sim\ 0.3$
A_F	$1.6 + 0.00056(m - 756)$

TABLE II
TYPICAL VALUE FOR CALCULATING AERO DRAG FORCE F_a IN (4), ADOPTED FROM [20].

II. VIRTUAL VEHICLE MODEL

A. Quarter Car Vehicle Dynamics

This section describes the quarter car model used in the virtual vehicle plant. More details can be found in [20], [21]. Consider the following quarter car longitudinal dynamics,

$$\dot{v}_x = \frac{n_w}{m} F_x - g \sin\sigma - \frac{1}{m} F_a \tag{1a}$$

$$\dot{\omega} = \frac{1}{I_w}\left(\frac{T}{n_w} - F_x R\right) \tag{1b}$$

where n_w is the number of driving wheels, which equals 2 for front/rear driving vehicle and 4 for all wheel drive configuration, σ is the road bank angle, I_w is the wheel rotational inertial, T is the total driving torque (as applied to all driving wheels) and F_x is the total tire force, as computed by the following Magic formula [22]

$$F_x = F_z D \sin\{C \arctan[Bs - E(Bs - \arctan(Bx))]\} \tag{2}$$

with the parameters B, C, D, E given in Table I. Note that F_z is normal force and s is slip ratio defined as

$$s = \frac{\omega R - v_x}{v_x} \tag{3}$$

with R being the wheel effective radius.

Finally, according to [20], the aerodynamic drag force F_a in (2) can be modeled by (assuming wind speed is 0):

$$F_a = \frac{1}{2}\rho C_d A_F v_x^2 \tag{4}$$

where ρ is the air mass density, C_d is the aerodynamic drag coefficient, A_F is the effective front area. Typical values for ρ, C_d and A_F are listed in Table II.

B. Driveline Dynamic

The closed loop driveline (electric motor and transmission) dynamic is modeled as a first order transfer function, as follows

$$G(s) = \frac{T}{T_c} = \frac{1}{T_d s + 1} \tag{5}$$

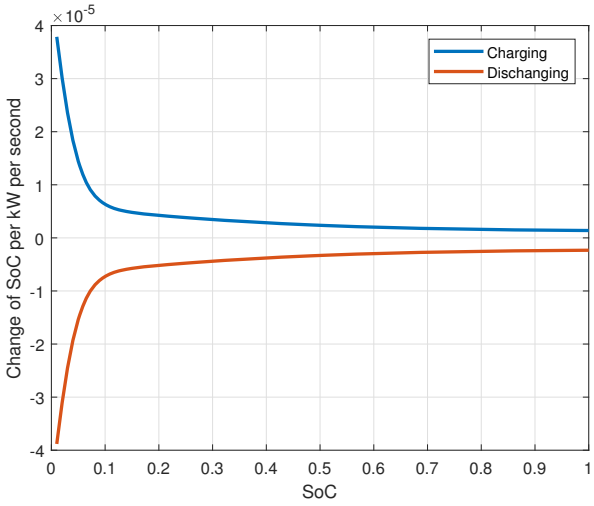

Fig. 1. SOC change rate $h(\zeta, P_b)$ when $P_b = 1$kW.

where T_c is the commanded wheel torque and T is the actual delivered value, and T_d represents the time constant of the driveline.

C. Nonlinear Battery Model

As will be seen shortly, MPC indirectly penalizes energy usage by minimizing wheel torque. In order to simulate the effectiveness of such approach, actual wheel torque T and wheel speed ω are converted into power charge/discharge command P_b to battery, and the battery state-of-charge (SOC) dynamic model is given as follows.

$$\dot{\zeta} = h(\zeta, P_b) \tag{6}$$

where ζ is the current battery SOC. Furthermore, in this study, a nonlinear battery SOC model is used, i.e., the right hand side $h(\zeta, P_b)$ of (6) is assumed to be nonlinear on ζ and linear on P_b. In particular, the nonlinear function (6) is specified by Figure 7, which is obtained by scaling the 3.2MWh battery presented in [23] to 66kWh.

D. FTP Driving Cycle

As mentioned earlier, EPA Federal Test Procedure (FTP) driving cycle is used to test the effectiveness and robustness of the MPC speed control. FTP driving cycle is commonly used for city driving testing, and includes an approximate driving distance of 17.77 km and average speed of 34.1 km/h [24]. Figure 2 plots the time profile of a typical FTP driving cycle. In this section, ten thousands synthetic FTP driving cycles are used to perform probabilistic analysis of the MPC control, which are generated by the autoregressive moving average model following the similar procedure as in [18]. In particular, Figure 3 plots a selected period of the FTP driving cycle, together with the standard deviation of the ten thousands cycles. Despite the variation introduced in the ten thousands driving cycles as demonstrated in Figure 3, the key statistic of each driving cycle still conform to a typical FTP cycle. For

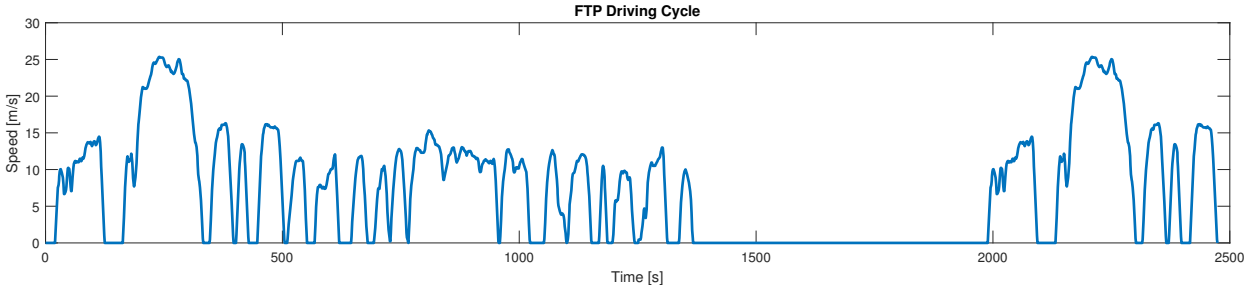

Fig. 2. FTP driving cycle.

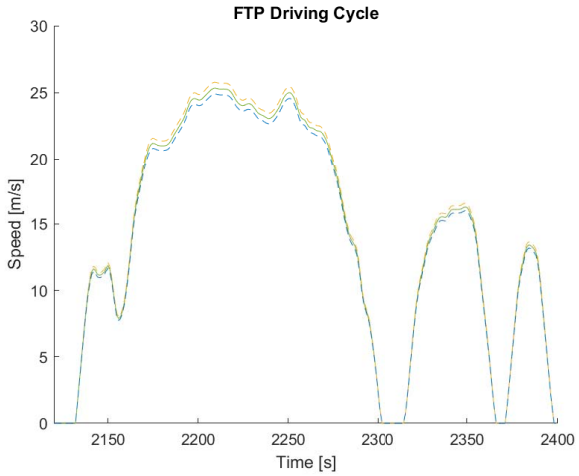

Fig. 3. Snapshot of FTP driving cycles with mean and standard deviation. Solid line: mean of the ten thousands cycles. Dotted line: Standard deviation.

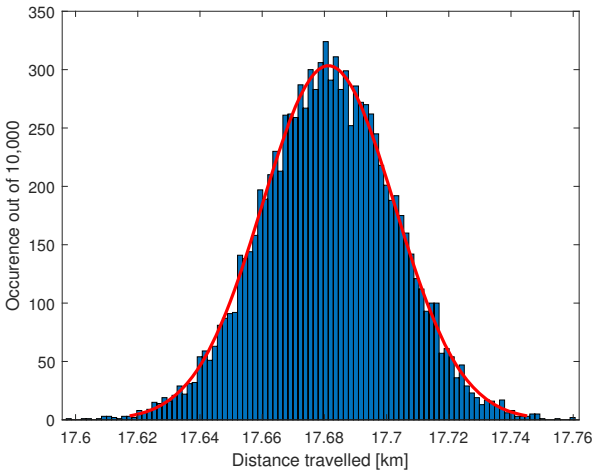

Fig. 4. Distance travelled of the synthetic FTP driving cycles.

example, Figure 4 plots the distribution of travelling distance of each cycle, with the red lines being the Gaussian distribution fitting that has a mean of 17.68 km and a standard deviation of 210 meters only.

III. MPC for Speed Tracking

This section details the prediction model used for MPC, followed by the formulation of a linear parametric varying MPC (LPV-MPC).

A. Model Linearization

Recall that model (1)-(4) is nonlinear. To simplify and linearize (1)-(4) for MPC to predict the system evolution and to compute optimal control action, one can assume that during the prediction steps the wheel is at steady state. In other words, throughout the prediction horizon

$$\dot{\omega} = 0$$

Therefore,

$$F_x = T/(n_w R)$$

and

$$\dot{v}_x = \frac{1}{m}\frac{T}{R} - g\sin\sigma - \frac{1}{m}F_a \tag{7}$$

Given nominal point (T_0, v_{x0}), (7) can be linearized as:

$$\begin{aligned}\delta\dot{v}_x =& \frac{1}{m}\frac{T_0}{R} - g\sin\sigma - \frac{1}{2m}\rho C_d A_F v_{x0}^2 \\ & - \frac{1}{m}\rho C_d A_F v_{x0}\delta v_x + \frac{1}{mR}\delta T\end{aligned} \tag{8}$$

which can be discretized into the following difference equation using Euler's method

$$\begin{aligned}\delta v_x(t+1) =& \delta v_x(t) \\ & + \left[\frac{1}{m}\frac{T_0}{R} - g\sin\sigma - \frac{1}{2m}\rho C_d A_F v_{x0}^2\right] T_s \\ & - \frac{1}{m}\rho C_d A_F v_{x0} T_s \delta v_x(t) + \frac{1}{mR} T_s \delta T(t) \\ =:& g(\delta v_x(t), \delta T(t))\end{aligned} \tag{9}$$

where T_s is the sampling time and t denotes current discrete time index.

Remark 1: Note that the simplification, linearization, and discretization discussed in this session is for MPC prediction

only, which will be utilized in the optimal control problem formulation presented shortly. For the virtual vehicle simulation, the full nonlinear model (1)-(4) is used.

B. Optimal Control Problem Formulation

At each sampling time t, the LPV-MPC linearized and discretize the nonlinear model to obtain the linearized prediction model (9) around the nominal operating point $(T(t), v_x(t))$, where $T(t)$ and $v_x(t)$ are feedback values. The following optimal control problem (OCP) is then formulated:

$$\min_{Z_t, U_t} \quad J(Z_t, U_t) = \sum_{k=1}^{p} \underbrace{|| v_x(t+k) - v_x^r(t+k)||^2_{Q_v}}_{\text{speed tracking}} + \sum_{k=0}^{p-1} \underbrace{||T(t+k)||^2_{Q_T}}_{\text{fuel consumption}} + \sum_{k=0}^{p} \underbrace{||T(t+k) - T(t+k-1)||^2_{Q_d}}_{\text{ride comfort}} \quad (10a)$$

$$\text{s.t.} \quad \delta v_x(t) = 0 \quad (10b)$$

$$\delta v_x(t+k) = g(\delta v_x(t+k-1), \delta T(t+k-1), \quad 1 \le k \le p \quad (10c)$$

$$v_x(t+k) = v_x(t) + \delta v_x(t+k), \quad 1 \le k \le p \quad (10d)$$

$$T(t+k) = T(t) + \delta T(t+k), 0 \le k \le p-1 \quad (10e)$$

$$T_{min} \le T(t+k) \le T_{max}, \quad 0 \le k \le p-1 \quad (10f)$$

$$\Delta_{min} \le T(t+k) - T(t+k-1) \le \Delta_{max}, \quad 0 \le k \le p-1 \quad (10g)$$

where $Z_t = \{v_x(t+1), \ldots, v_x(t+p)\}$ and $U_t = \{Tt, \ldots, Tt+p-1\}$ are the state and input trajectory over prediction horizon, which are to be optimized, and $v_x^r(t+k)$, $k = 1, \ldots, p$ are the state reference for tracking. The OCP (10) has three parameters to be calibrated, namely Q_v, Q_T, and Q_d. Specifically,

- Q_v penalizes speed tracking error;
- Q_T imposes a cost for driving torque and consequently imposes a cost on energy consumption; and finally
- Q_d ensures the smoothness of input trajectory by penalizing the variation of driving torque. Note that by suppressing the variation of driving torque, one also decreases the jerk (rate of change of acceleration) and improves ride comfort.

Remark 2: It is trivial to see that the above OCP can be translated into linear constrained quadratic programming (QP) problems, and can be solved in real-time by embedded devices [2], [3], [25], [26].

IV. Numerical Results and Discussion

This section presents numerical results concerning the MPC speed control presented above. The numerical values for various parameters are summarized in Table III. Recall from previous section that ten thousands synthetic FTP driving cycles, as plotted in Figures 3 and 4 are used for simulation.

Parameter	Value
$m\ [kg]$	1500
n_w [-]	2
$R\ [m]$	0.2159
μ_i [-]	1
Q_v [-]	10
Q_T [-]	0.001
Q_d [-]	1
$T_{max}\ [Nm]$	500
$T_{min}\ [Nm]$	-500
$\Delta_{max}\ [Nm]$	70
$\Delta_{min}\ [Nm]$	-200
$T_s\ [ms]$	100
$T_d\ [ms]$	300

TABLE III
PARAMETERS FOR THE QUARTER CAR MODEL AND MPC.

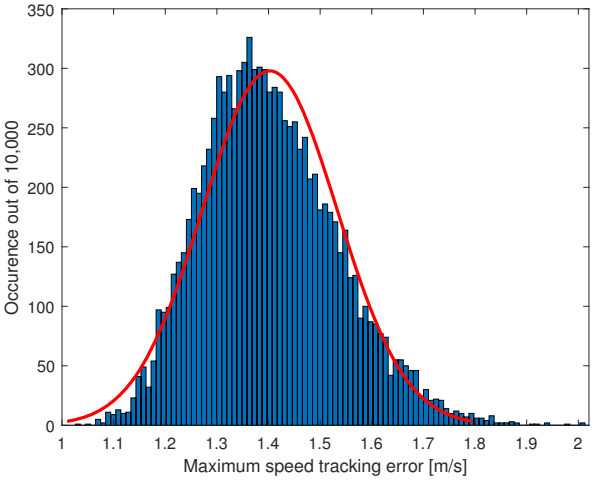

Fig. 5. Maximum speed tracking error.

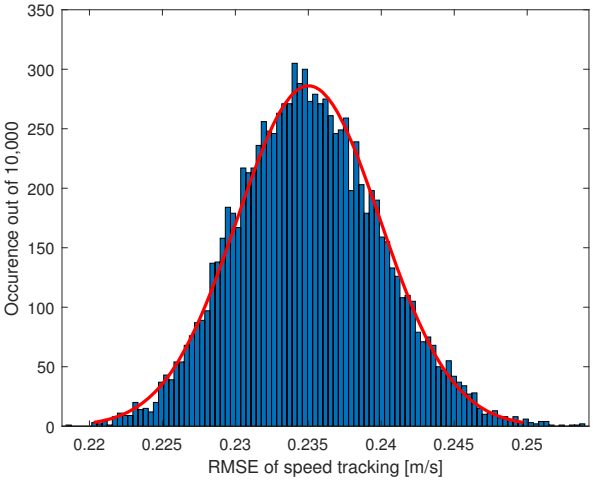

Fig. 6. RMSE of speed tracking.

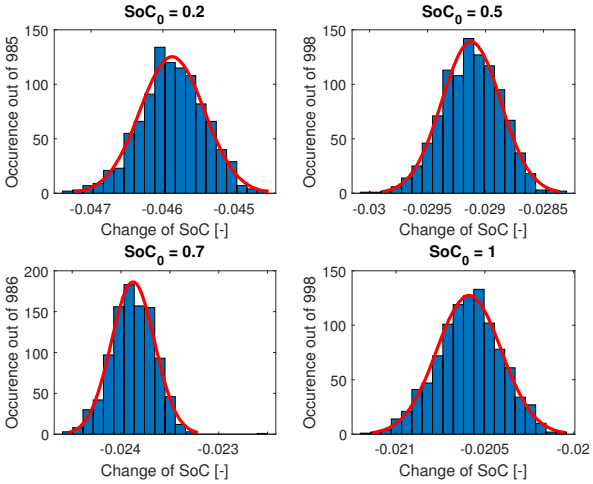

Fig. 7. Change of battery SOC

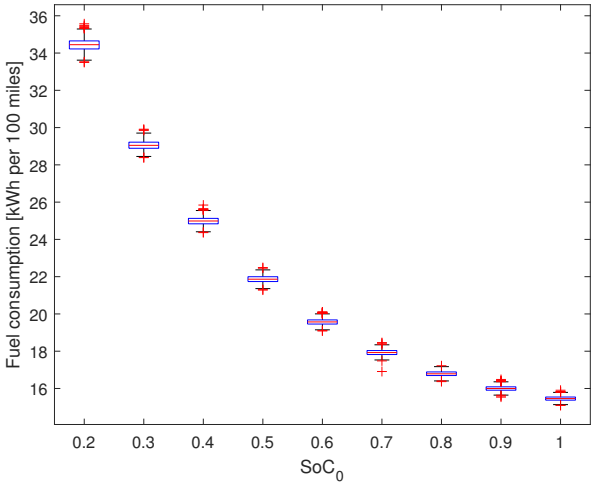

Fig. 9. Box plot of energy consumption for various SOC_0.

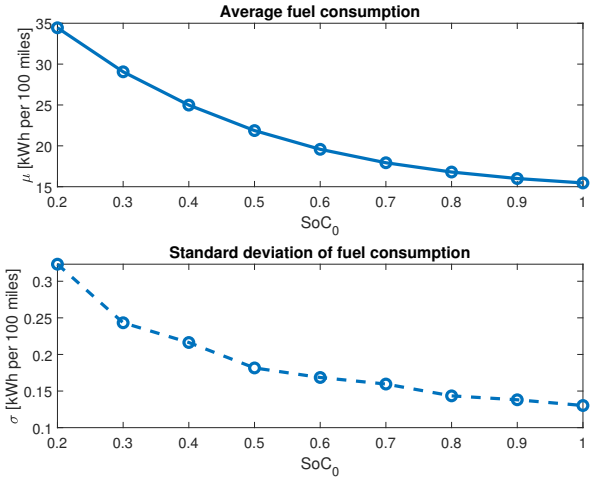

Fig. 8. Energy consumption for various SOC_0.

The MPC speed tracking results are summarized in Figures 5 and 6, with the red lines being the Gaussian distribution fitting. In particular, the distribution of maximum speed tracking error is skewed towards left, and its Gaussian fit has a mean of 1.402 m/s and standard deviation of 0.131 m/s. The effectiveness of MPC speed control is proven by the root-mean-square-error (RMSE), which has a mean of only 0.235 m/s and standard deviation of 0.005 m/s. Note that these results provide an intuitive view of the robustness of MPC speed tracking over FTP driving cycle. A robust MPC design can be developed to ensure the worst case performance is satisfactory; however, the tight deviation in Figure 6 suggests that such controller design may be over-restrictive.

The energy efficiency is simulated by utilizing the nonlinear battery SOC model (6). The initial SOC, denoted as SOC_0, is randomly generated among $0.2, 0.3, \ldots, 1$. Therefore, for each SOC_0, the number of driving cycles being simulated can be different. Figure 7 plots the change of SOC after FTP cycle completion, for the cases of SOC_0 equaling 0.2, 0.5, 0.7, and 1. It can be seen that as the initial SOC decreases, the change of SOC throughout the cycle increases, indicating that the battery is operating in less efficient region as more energy are required to drive the similar cycle. This can also be demonstrated by Figures 8 and 9, which plot, for various SOC_0, the energy efficiency (mean/deviation and box plot) in terms of kWh per 100 miles. It is worth noting that when initial SOC increases, not only the power consumption drops but also its standard deviation, indicating higher robustness when operating in higher SOC region. These results also suggest to operate the EV in higher battery SOC mode, not only to preserve higher efficiency but also to maintain better resiliency.

V. Conclusion

This paper conducts a probabilistic analysis of energy consumption of electric vehicle, which is under speed control mode by a MPC controller. In particular, a quarter car model is used by MPC for prediction and control action optimization, and battery is modeled by nonlinear dynamic equation. The speed tracking accuracy and fuel economy of the MPC are evaluated on ten thousands synthetic FTP driving cycles. The robustness of MPC speed control is demonstrated, and insights on energy consumption and battery operations are discussed. In particular, it is more energy efficient and more robust to operate in higher SOC region. This work lay out a framework to investigate EV speed control and fuel efficiency *probabilistically*. Future work includes using a higher fidelity vehicle model as virtual plant. The interaction of EV with other energy consumption units, such as quadrocopter [27], water processing plant [28], and renewable energy systems [29], [30], are also future work directions.

Acknowledgment

This work is supported in part by faculty startup fund from School of Engineering and Computer Science at Oakland

University.

REFERENCES

[1] D. Q. Mayne, M. M. Seron, and S. Raković, "Robust model predictive control of constrained linear systems with bounded disturbances," *Automatica*, vol. 41, no. 2, pp. 219–224, 2005.

[2] A. Bemporad, D. Bernardini, R. Long, and J. Verdejo, "Model predictive control of turbocharged gasoline engines for mass production," SAE Technical Paper, Tech. Rep., 2018.

[3] A. Bemporad, D. Bernardini, M. Livshiz, and B. Pattipati, "Supervisory model predictive control of a powertrain with a continuously variable transmission," SAE Technical Paper, Tech. Rep., 2018.

[4] S. Di Cairano, H. E. Tseng, D. Bernardini, and A. Bemporad, "Vehicle yaw stability control by coordinated active front steering and differential braking in the tire sideslip angles domain," *IEEE Transactions on Control Systems Technology*, vol. 21, no. 4, pp. 1236–1248, 2012.

[5] Y. Shi, H. D. Tuan, A. V. Savkin, T. Q. Duong, and H. V. Poor, "Model predictive control for smart grids with multiple electric-vehicle charging stations," *IEEE Transactions on Smart Grid*, vol. 10, no. 2, pp. 2127–2136, 2018.

[6] T. Jin, J. Guo, M. A. Mohamed, and M. Wang, "A novel model predictive control via optimized vector selection method for common-mode voltage reduction of three-phase inverters," *IEEE Access*, vol. 7, pp. 95 351–95 363, 2019.

[7] G.-P. Liu, "Predictive control of networked nonlinear multiagent systems with communication constraints," *IEEE Transactions on Systems, Man, and Cybernetics: Systems*, 2018.

[8] H. Wi, H. Park, and D. Hong, "Model predictive longitudinal control for heavy-duty vehicle platoon using lead vehicle pedal information," *International Journal of Automotive Technology*, vol. 21, no. 3, pp. 563–569, 2020.

[9] Y. Mizushima, I. Okawa, and K. Nonaka, "Model predictive control for autonomous vehicles with speed profile shaping," *IFAC-PapersOnLine*, vol. 52, no. 8, pp. 31–36, 2019.

[10] J. A. Matute, M. Marcano, A. Zubizarreta, and J. Perez, "Longitudinal model predictive control with comfortable speed planner," in *2018 IEEE International Conference on Autonomous Robot Systems and Competitions (ICARSC)*. IEEE, 2018, pp. 60–64.

[11] F. Hoekstra, L. W. Ribelles, H. Bergveld, and M. Donkers, "Real-time range maximisation of electric vehicles through active cell balancing using model-predictive control," in *2020 American Control Conference*. IEEE, 2020.

[12] S. Di Cairano, D. Bernardini, A. Bemporad, and I. V. Kolmanovsky, "Stochastic mpc with learning for driver-predictive vehicle control and its application to hev energy management," *IEEE Transactions on Control Systems Technology*, vol. 22, no. 3, pp. 1018–1031, 2013.

[13] A. Nahidi and et al, "Modular integrated longitudinal and lateral vehicle stability control for electric vehicles," *Mechatronics*, vol. 44, pp. 60–70, 2017.

[14] J. Wurts, J. Dallas, J. L. Stein, and T. Ersal, "Adaptive nonlinear model predictive control for collision imminent steering with uncertain coefficient of friction," in *2020 ACC*, 2020.

[15] M. V. Kothare, V. Balakrishnan, and M. Morari, "Robust constrained model predictive control using linear matrix inequalities," *Automatica*, vol. 32, no. 10, pp. 1361–1379, 1996.

[16] D. Bernardini and A. Bemporad, "Stabilizing model predictive control of stochastic constrained linear systems," *IEEE Transactions on Automatic Control*, vol. 57, no. 6, pp. 1468–1480, 2011.

[17] N. Li, I. Kolmanovsky, and A. Girard, "Model-free optimal control based automotive control system falsification," in *2017 American Control Conference (ACC)*. IEEE, 2017, pp. 636–641.

[18] J. Chen and C. Rabiti, "Synthetic wind speed scenarios generation for probabilistic analysis of hybrid energy systems," *Energy*, vol. 120, pp. 507–517, 2017.

[19] C. Rabiti, A. Alfonsi, J. Cogliati, D. Mandelli, R. Kinoshita, S. Sen, C. Wang, P. W. Talbot, D. P. Maljovec, and J. Chen, "Raven user manual," Idaho National Lab.(INL), Idaho Falls, ID (United States), Tech. Rep., 2017.

[20] R. Rajamani, *Vehicle dynamics and control*. Springer Science & Business Media, 2011.

[21] P. Falcone, M. Tufo, F. Borrelli, J. Asgari, and H. E. Tseng, "A linear time varying model predictive control approach to the integrated vehicle dynamics control problem in autonomous systems," in *2007 46th IEEE Conference on Decision and Control*. IEEE, 2007, pp. 2980–2985.

[22] E. Bakker, L. Nyborg, and H. B. Pacejka, "Tyre modelling for use in vehicle dynamics studies," *SAE Transactions*, pp. 190–204, 1987.

[23] D. Wu, P. Balducci, A. Crawford, V. Viswanathan, and M. Kintner-Meyer, "Optimal control for battery storage using nonlinear models," in *Proc. EESAT Conf*, 2017.

[24] Wikipedia, "FTP-75," https://en.wikipedia.org/wiki/FTP-75.

[25] G. Cimini and A. Bemporad, "Exact complexity certification of active-set methods for quadratic programming," *IEEE Transactions on Automatic Control*, vol. 62, no. 12, pp. 6094–6109, 2017.

[26] J. Nocedal and S. Wright, *Numerical optimization*. Springer Science & Business Media, 2006.

[27] M. W. Mueller and R. D'Andrea, "Stability and control of a quadrocopter despite the complete loss of one, two, or three propellers," in *2014 IEEE international conference on robotics and automation (ICRA)*. IEEE, 2014, pp. 45–52.

[28] J. S. Kim, J. Chen, and H. E. Garcia, "Modeling, control, and dynamic performance analysis of a reverse osmosis desalination plant integrated within hybrid energy systems," *Energy*, vol. 112, pp. 52–66, 2016.

[29] H. E. Garcia, J. Chen, J. S. Kim, R. B. Vilim, W. R. Binder, S. M. B. Sitton, R. D. Boardman, M. G. McKellar, and C. J. Paredis, "Dynamic performance analysis of two regional nuclear hybrid energy systems," *Energy*, vol. 107, pp. 234–258, 2016.

[30] J. Chen and H. E. Garcia, "Economic optimization of operations for hybrid energy systems under variable markets," *Applied Energy*, vol. 177, pp. 11–24, 2016.